

Bose-Einstein condensate in an optical lattice with tunable spacing: transport and static properties

Leonardo Fallani, Chiara Fort, Jessica E. Lye and Massimo Inguscio

*LENS European Laboratory for Nonlinear Spectroscopy,
Dipartimento di Fisica - Università di Firenze, and INFN,
via Nello Carrara 1, I-50019 Sesto Fiorentino (FI), Italy*
fallani@lens.unifi.it

Abstract: In this Letter we report the investigation of transport and static properties of a Bose-Einstein condensate in a large-spaced optical lattice. The lattice spacing can be easily tuned starting from few micrometers by adjusting the relative angle of two partially reflective mirrors. We have performed *in-situ* imaging of the atoms trapped in the potential wells of a 20 μm spaced lattice. For a lattice spacing of 10 μm we have studied the transport properties of the system and the interference pattern after expansion, evidencing quite different results with respect to the physics of BECs in ordinary near-infrared standing wave lattices, owing to the different length and energy scales.

OCIS codes: (020.0020) Atomic and molecular physics; (020.7010) Trapping

References and links

1. B. P. Anderson and M. A. Kasevich, "Macroscopic Quantum Interference from Atomic Tunnel Arrays," *Science* **282**, 1686–1689 (1998).
2. F. S. Cataliotti, S. Burger, C. Fort, P. Maddaloni, F. Minardi, A. Trombettoni, A. Smerzi, and M. Inguscio, "Josephson Junction Arrays with Bose-Einstein Condensates," *Science* **293**, 843–846 (2001).
3. M. Greiner, O. Mandel, T. Esslinger, T. W. Hänsch, and I. Bloch, "Quantum phase transition from a superfluid to a Mott insulator in a gas of ultracold atoms," *Nature* **415**, 39–44 (2002).
4. G. K. Brennen, C. M. Caves, P. S. Jessen, and I. H. Deutsch, "Quantum Logic Gates in Optical Lattices," *Phys. Rev. Lett.* **82**, 1060–1063 (1999).
5. D. Jaksch, H.-J. Briegel, J. I. Cirac, C. W. Gardiner, and P. Zoller, "Entanglement of Atoms via Cold Controlled Collisions," *Phys. Rev. Lett.* **82**, 1975–1978 (1999).
6. O. Mandel, M. Greiner, A. Widera, T. Rom, T. W. Hänsch, and I. Bloch, "Controlled collisions for multi-particle entanglement of optically trapped atoms," *Nature* **425**, 937–940 (2003).
7. D. Schrader, I. Dotsenko, M. Khudaverdyan, Y. Miroshnychenko, A. Rauschenbeutel, and D. Meschede, "Neutral Atom Quantum Register," *Phys. Rev. Lett.* **93**, 150501 (2004).
8. R. Scheunemann, F. S. Cataliotti, T. W. Hänsch, and M. Weitz, "Resolving and addressing atoms in individual sites of a CO₂-laser optical lattice," *Phys. Rev. A* **62**, 051801(R) (2000).
9. R. Dumke, M. Volk, T. Müther, F. B. J. Buchkremer, G. Birkl, and W. Ertmer, "Micro-optical Realization of Arrays of Selectively Addressable Dipole Traps: A Scalable Configuration for Quantum Computation with Atomic Qubits," *Phys. Rev. Lett.* **89**, 097903 (2002).
10. O. Morsch, J. H. Müller, M. Cristiani, D. Ciampini, and E. Arimondo, "Bloch Oscillations and Mean-Field Effects of Bose-Einstein Condensates in 1D Optical Lattices," *Phys. Rev. Lett.* **87**, 140402 (2001).
11. S. Peil, J. V. Porto, B. Laburthe Tolra, J. M. Obrecht, B. E. King, M. Subbotin, S. L. Rolston, and W. D. Phillips, "Patterned loading of a Bose-Einstein condensate into an optical lattice," *Phys. Rev. A* **67**, 051603(R) (2003).
12. Z. Hadzibabic, S. Stock, B. Battelier, V. Bretin, and J. Dalibard, "Interference of an Array of Independent Bose-Einstein Condensates," *Phys. Rev. Lett.* **93**, 180403 (2004).
13. M. Greiner, I. Bloch, O. Mandel, T. W. Hänsch, and T. Esslinger, "Exploring Phase Coherence in a 2D Lattice of Bose-Einstein Condensates," *Phys. Rev. Lett.* **87**, 160405 (2001).

14. P. Pedri, L. Pitaevskii, S. Stringari, C. Fort, S. Burger, F. S. Cataliotti, P. Maddaloni, F. Minardi, and M. Inguscio, "Expansion of a Coherent Array of Bose-Einstein Condensates," *Phys. Rev. Lett.* **87**, 220401 (2001).
 15. W. Zwerger, "MottHubbard transition of cold atoms in optical lattices," *J. Opt. B* **5** S9–S16 (2003).
 16. M. R. Andrews, C. G. Townsend, H.-J. Miesner, D. S. Durfee, D. M. Kurn, and W. Ketterle, "Observation of Interference Between Two Bose Condensates," *Science* **275**, 637–641 (1997).
 17. J. E. Lye, L. Fallani, M. Modugno, D. Wiersma, C. Fort, and M. Inguscio, "A Bose-Einstein condensate in a random potential," preprint arXiv:cond-mat/0412167 (2004).
-

1. Introduction

In the last few years Bose-Einstein condensates (BECs) in optical lattices have been the subject of extremely intense and rewarding research, both theoretical and experimental. Periodic potentials produced with near-infrared standing waves have been used to investigate the transport and superfluid properties of Bose-condensed samples [1, 2], as well as to study effects correlated with the physics of strongly correlated many-body systems [3]. Ultracold atoms in optical lattices are also good candidates for the implementation of quantum computational schemes [4, 5]. In this respect, quantum logic operations have already been performed via cold controlled collisions on entangled sets of atoms trapped in a three-dimensional optical lattice [6]. In a recent experiment a one-dimensional lattice partially filled with atoms has been used to create a quantum register with the capability of single atom manipulation and detection [7]. In this context, a larger spacing optical lattice could simplify the fundamental goal of single-site addressability, that is hard to achieve in a traditional near-infrared standing-wave lattice. One possible approach consists in the realization of standing waves with CO₂ lasers emitting at 10 μm wavelength [8]. Even if CO₂ lattices provide the advantage of a complete suppression of heating mechanisms (due to the huge detuning from the atomic resonance), they present the drawback of a difficult experimental manipulation. A different approach involves the realization of arrays of dipole traps obtained by shining a far detuned laser beam onto a microfabricated array of microlenses [9]. Optical lattices with a spacing of few μm can also be obtained from the interference of two near-infrared laser beams intersecting at a small angle [10, 11, 12]. In the frame of this idea, in this Letter we present a simple system for the creation and the detection of optical lattices with spacing starting from $\approx 8 \mu\text{m}$, almost 20 times larger than the spacing of a traditional standing wave lattice, still using near-infrared light produced by solid state laser sources. The appeal of this system resides in the possibility to easily detect the lattice intensity profile and to accomplish a fine tuning of the lattice spacing simply by adjusting the relative angle of two partially reflective mirrors. We have investigated both static and dynamic properties of an ⁸⁷Rb BEC loaded in such a potential, evidencing quite different results with respect to the physics of ordinary lattices, caused by the different length and energy scales.

2. Experimental setup

The experimental setup for the production and the detection of the large spacing optical lattice is schematically shown in Fig. 1. A collimated laser beam coming from a Ti:Sa laser is shone onto a pair of partially reflective mirrors placed with a small relative angle δ one in front of the other at a distance of $\approx 1 \text{ mm}$. As shown in Fig. 1, the multiple reflection of the laser beam from these mirrors produces, at the second order of reflection, two separate beams (of different intensities) with a relative angle 2δ . These two beams, following different optical paths, are then guided by a lens system to recombine onto the condensate, where they interfere producing a periodic pattern with alternating intensity maxima and minima. The period d of this lattice, that is oriented along the difference of the wavevectors, depends on the angle α between the beams according to

$$d = \frac{\lambda}{2 \sin(\alpha/2)}. \quad (1)$$

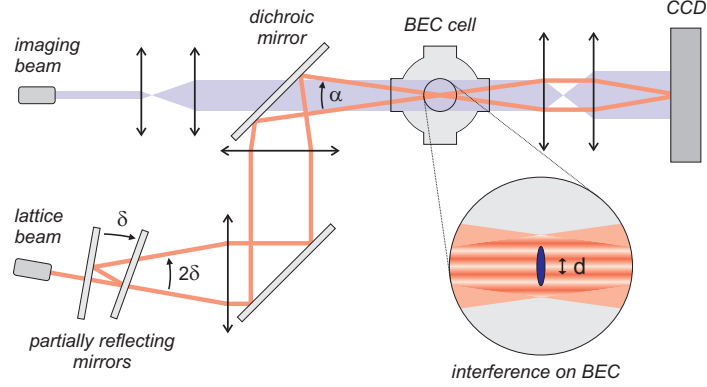


Fig. 1. Optical setup for the production and detection of a large spacing optical lattice. The two beams creating the interference pattern are obtained from the multiple reflections of a laser beam by a pair of partially reflective mirrors placed with a relative angle one in front of the other. The lattice spacing d can be tuned by changing the angle δ between the two partially reflecting mirrors. The vertical axis is orthogonal to the page.

It is easy to show that in the case of counterpropagating beams ($\alpha = \pi$) the above expression reduces to the well known spacing $\lambda/2$ for a standing wave lattice. In the other limit, when the two beams are almost copropagating ($\alpha \simeq 0$), d may become very large. In our setup, varying the angle δ between the two mirrors, it is possible to easily adjust the lattice spacing to the desired value. For the working wavelength $\lambda = 820$ nm the lower limit is $d \approx 8 \mu\text{m}$, corresponding to the maximum angle $\alpha = 25^\circ$ that is possible to reach in our setup taking into account the finite size of the vacuum cell windows. Since the two beams producing the lattice do not have the same intensity, we expect the resulting interference pattern to show a reduced contrast with respect to the case in which the two beams have the same intensity. It can be shown that the intensity of the lattice I_L , i.e. the intensity difference between constructive interference and destructive interference, is given by

$$I_L = I_{max} - I_{min} = 4t^2(1-t)I_0, \quad (2)$$

where t is the transmissivity of the partially reflecting mirrors and I_0 is the intensity of the beam incident on them. It is easy to show that this expression has a maximum for $t = 2/3$. For this reason in the experiment we have used mirrors with $t \simeq 0.7$, corresponding to the maximum lattice intensity $I_L \simeq 0.59I_0$ achievable with this technique.

An appealing feature of the system shown in Fig. 1 is that the lattice beams are aligned quasi-parallel to the radial horizontal axis of the condensate, following the same path of the imaging beam used in our setup. This has been made possible by the use of a dichroic mirror, reflecting in the range $\lambda > 800$ nm and transmitting in the range $\lambda < 800$ nm. This feature allows us to use the same imaging setup to detect both the BEC and the spatial profile of the lattice light intensity. This means that we can image in consecutive photos both the condensate and the exact potential that the condensate experiences. Indeed, since the CCD plane is conjugate to the vertical plane passing through the trap axis, the intensity profile recorded by the CCD is exactly the same (except for a magnification factor) as the one imaged onto the condensate. Furthermore, by calibrating the CCD responsivity with a reference beam of known intensity, it is possible to convert the digitized signal of each pixel into an intensity value and thus calculate the height of the potential V_0 . In the following, the lattice height and the other energy scales

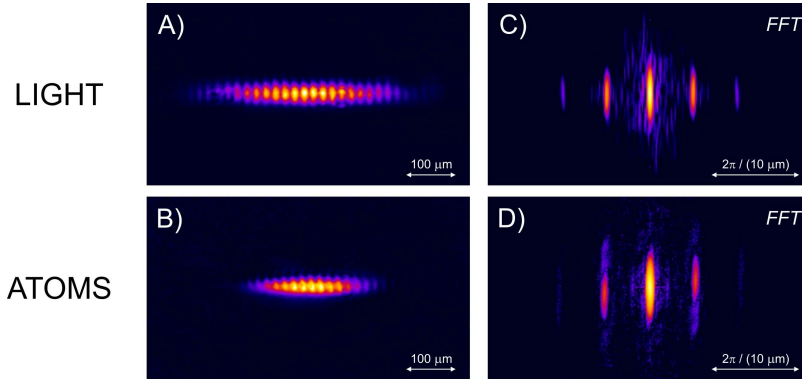


Fig. 2. An optical lattice with $d = 20 \mu\text{m}$ spacing. In the top row we show the intensity distribution of the light recorded by the CCD (a) and the corresponding Fourier transform (c). In the bottom row we show the density distribution (b) of the atoms trapped in the lattice sites imaged *in situ* a few μs after switching off the lattice, together with its Fourier transform (d), showing well resolved peaks in the same position as the ones in (c).

will be conveniently expressed in frequency units (using the implicit assumption of a division by the Planck constant \hbar).

To illustrate the advantages of this imaging setup, in Fig. 2(a) we show the intensity profile of an optical lattice with spacing $d = 20 \mu\text{m}$, while in Fig. 2(b) we show an absorption image of the atoms trapped in the potential wells of the same lattice. The experimental sequence used to trap the atoms in the optical lattice and to image *in situ* the atomic distribution is the following. First we produce a cigar-shaped BEC of ^{87}Rb in a Ioffe-Pritchard magnetostatic trap, with trap frequencies $\omega_z/2\pi = 8.74(1)$ Hz along the symmetry axis z (oriented horizontally) and $\omega_r/2\pi = 85(1)$ Hz along the orthogonal directions. The typical diameter of the condensates is $150 \mu\text{m}$ axially and $15 \mu\text{m}$ radially. We note that the lattice beam profile has been tailored with cylindrical lenses in order to match the condensate elongated shape (see Fig. 2(a)). After producing the BEC, still maintaining the magnetic confinement, we ramp in 100 ms the height of the lattice from zero to the final value by using an acousto-optic modulator (AOM). After the end of the ramp we wait 50 ms, then we abruptly switch off the optical lattice with the same AOM and, after a few tens of μs , we flash the imaging beam for the detection phase. The latter time interval is necessary not to perturb the imaging with lattice light coming onto the CCD, but is small enough not to let the atoms expand from the lattice sites once the optical confinement is released. The combination of the CCD electronic shutter and an interferential bandpass filter placed in front of the camera (centered around $\lambda = 780$ nm) allows a complete extinction of the lattice light at the time of acquisition. In Fig. 2(c) and 2(d) we show, respectively, the power spectrum of the two-dimensional Fourier transform of the distributions shown in Figs. 2(a) and 2(b). As one can see, both the distributions are characterized by sharp peaks in momentum space: from the position of these peaks it is possible to precisely measure the spatial period of the observed structures.

In Fig. 3 we show *in situ* images of the atomic sample for different lattice spacings ranging from $20 \mu\text{m}$ to $80 \mu\text{m}$. The different spacings are obtained, as shown before, by simply changing the angle δ between the mirrors shown in Fig. 1.

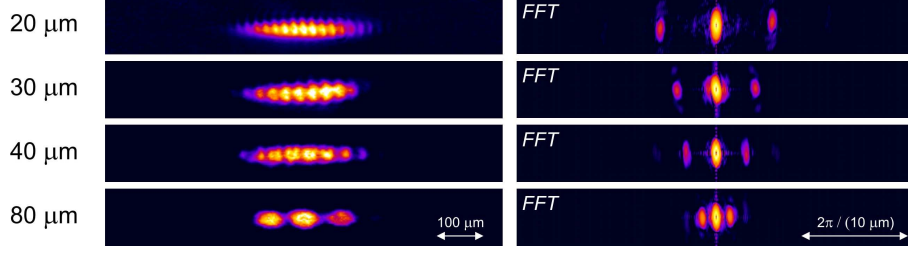


Fig. 3. *In situ* images of the atoms trapped in the lattice sites (left) and Fourier transform of the density distribution (right) for different lattice spacings from 20 to 80 μm . The different spacings have been obtained by changing the angle δ between the mirrors shown in Fig. 1.

3. Static properties

With the usual near-infrared standing-wave lattices employed so far in many experiments it is not possible to optically resolve *in situ* the modulation of the atomic density distribution, since the distance between lattice sites is typically less than 1 μm . As a matter of fact, in most of the cases the diagnostic of the system is carried out by looking at the atomic gas after expansion. This kind of analysis provides useful information on the quantum nature of the system. When the height of the optical lattice is larger than the chemical potential (tight binding regime), the system forms an array of condensates localized in the wells of the periodic potential. It has been experimentally observed that such an array of coherent atomic states, once released from the trap, produces after expansion a periodic interference pattern [3, 13, 14]. The high contrast interference observed in these experiments has been related to the long range coherence that exists in the superfluid regime when the tunnelling rate between neighboring sites is sufficiently large. Since the tunnelling rate strongly depends on the lattice spacing d (being proportional to e^{-2d}/\sqrt{d} in the tight binding regime [15]), it is worth studying the expansion of the BEC from a large-spaced lattice, in which tunnelling is expected to be exponentially suppressed.

Let us consider a linear array of condensates trapped in an optical lattice with spacing d . After releasing the atoms from the trapping potential one expects to observe a periodic interference pattern with spacing

$$d' = \frac{ht_{exp}}{md}, \quad (3)$$

where m is the atomic mass, t_{exp} is the expansion time and d is the spacing of the optical lattice [16]. We have studied the expansion from a lattice with $d = 10 \mu\text{m}$, producing after $t_{exp} = 28$ ms an interference pattern with fringe spacing $d' = 12.8 \mu\text{m}$, easily detectable with our imaging setup. We note that for this lattice spacing the recoil energy $E_R = h^2/8md^2$, the natural energy scale for measuring the lattice height, is only 6 Hz, almost 600 times smaller than the recoil energy for a regular standing-wave lattice with $d = 0.4 \mu\text{m}$ spacing.

In the experiment, after producing the BEC, we ramp in 100 ms the intensity of the lattice beam from zero to different final values, then we wait 50 ms and suddenly switch off both the magnetic trap and the optical lattice, as indicated in Fig. 4(a). In Fig. 4(b) we show absorption images of the atomic density distribution after 28 ms of free expansion (left) together with their Fourier transform evaluated along the lattice axis (right) for different values of the lattice height ranging from $V_0 = 0$ to $V_0 = 4.6$ kHz. Increasing the lattice height above ~ 500 Hz we note that interference fringes with the expected spacing $d' \simeq 13 \mu\text{m}$ start to form, as indicated by the emergence of peaks in the Fourier transform, and their visibility increases with increasing lattice height. At the same time, the axial width of the overall distribution gets larger as a consequence

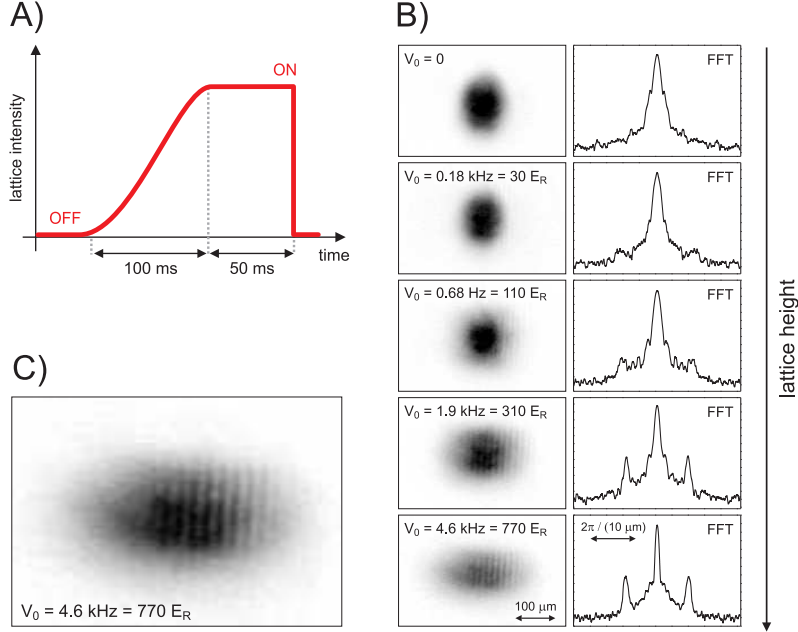


Fig. 4. Expansion from an optical lattice with $10 \mu\text{m}$ spacing. a) The intensity of the lattice is increased adiabatically from zero to the final value in 100 ms, then after 50 ms the lattice is abruptly switched off together with the harmonic trapping potential. b) Absorption images after 28 ms of expansion (left) and corresponding Fourier transform (right) for different lattice heights V_0 . c) Expanded density profile for $V_0 = 4.6 \text{ kHz}$: we observe the clear presence of interference fringes.

of the increased axial confinement in the lattice wells, that produces a faster expansion along the lattice direction. In Fig. 4(c) we show the interference pattern observed for the maximum lattice height $V_0 = 4.6 \text{ kHz}$, in which the system is deeply in the tight binding regime and we expect the BEC to be split into an array of condensates located in the lattice wells (the BEC chemical potential in the harmonic trap is $\mu \simeq 1 \text{ kHz}$). However, differently from [14], for this large spacing the tunnelling between neighboring sites is totally suppressed and the states in the different wells do not communicate one with each other. As a consequence, each state will evolve in time independently, according to its energy, that is different from site to site due to the inhomogeneity of the sample. In this situation we are observing interference fringes from an array of phase uncorrelated matter-wave sources, as recently reported in [12] with a similar system.

To get more insight into the problem of interference from uncorrelated sources, let us write down a very simple model. Following an obvious analogy with optics, we consider a linear array of point-like radiation sources disposed along \hat{z} with uniform spacing d , all emitting isotropically in space with the same amplitude. This problem is the extension of the Young's double slit experiment to the case of N emitters. We indicate the position of the sources along \hat{z} and their phases with the variables $\{z_n, \phi_n\}$. Let us suppose that we measure the field distribution on a screen parallel to \hat{z} , placed at a distance D from the emitters. The field amplitude, as a function of the position z' on the screen, is proportional to a sum of phase-factors describing

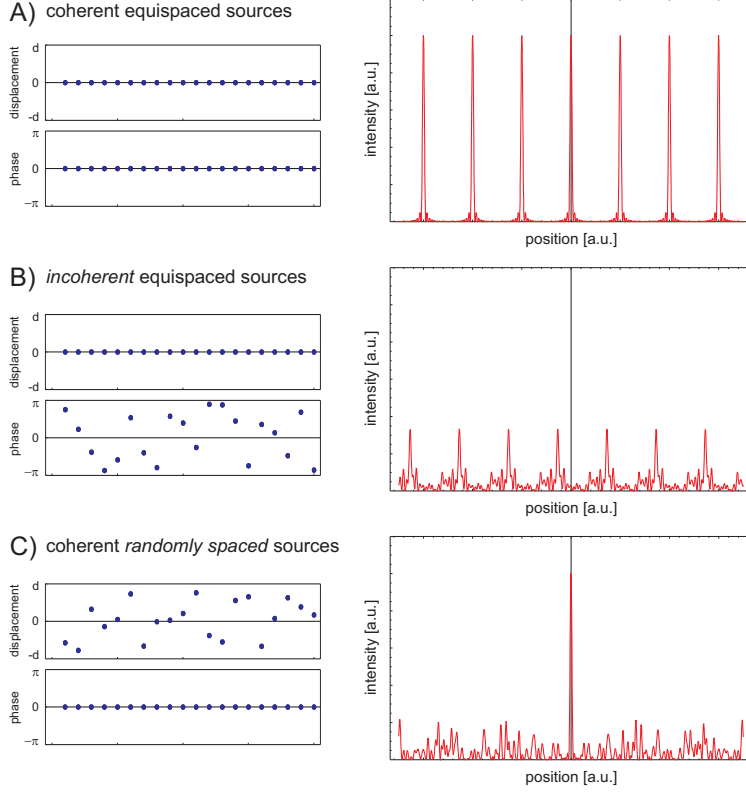


Fig. 5. Far-field intensity obtained from the interference of a linear chain of 20 point-like emitters. On the left of each row the diagrams show the particular set of positions and phases of the sources used to calculate, with Eq. (6), the interferograms shown on the right. The three sets refer to: a) uniform phase and uniform spacing; b) random phase and uniform spacing; c) uniform phase and random spacing.

the wave propagation in space:

$$A(z') \propto \sum_n e^{i(\phi_n + kd_n)}, \quad (4)$$

where k is the modulus of the wavevector and $d_n = \sqrt{D^2 + (z_n - z')^2}$ is the distance of the n -th source from the detection point. If one assumes that $D \gg (z_n - z')$, i.e. that we are observing the interference in the far-field, we can make the following approximation

$$d_n = \sqrt{D^2 + (z_n - z')^2} \simeq D \left[1 + \frac{1}{2} \left(\frac{z_n - z'}{D} \right)^2 \right]. \quad (5)$$

Using this assumption, the total intensity on the screen will be given by

$$|A(z')|^2 \propto \left| \sum_n e^{i(\phi_n + \frac{k}{2D}(z_n - z')^2)} \right|^2. \quad (6)$$

This quantity is evaluated numerically in Fig. 5 for $N = 20$ sources identified by three different sets of variables $\{z_n, \phi_n\}$, in which we release one at a time the hypothesis of identical phases

and uniform spacing. The diagrams on the left show the displacement of each source $\delta z_n = z_n - nd$ from the regular lattice position and its phase ϕ_n . The graphs on the right show the field intensity $|A(z')|^2$ calculated with Eq. (6).

In Fig. 5(a) we consider the ideal case of equispaced sources all emitting in phase. In this situation we observe a high-contrast interference pattern characterized by well resolved peaks at a distance inversely proportional to the distance d between the sources. In optics, this is the intensity distribution produced by a diffraction grating illuminated by coherent light. In matter-wave optics, a similar interferogram is observed in the superfluid regime after the expansion of BECs released from optical lattices produced with near-infrared standing waves [14]. Working out a slightly more realistic model, in which the finite size of the emitters is taken into account, the interferogram should be convolved with the diffraction figure from a single source, resulting in a decreased visibility of the higher order peaks.

In Fig. 5(b) we consider the case of equispaced sources with random phases. The interferogram on the right corresponds to the randomly generated set of phases shown on the left. In this case, even if no coherence is present across the array, we can still observe a periodic structure in the interferogram. This is indeed what we observe in Fig. 4(c) and what has been studied, both theoretically and experimentally, in [12]. We note that this periodic interference is produced in a single shot. Actually, averaging the intensity distribution over many different realizations, the contrast of the interferogram is expected to rapidly vanish, since the uncorrelated phases produce a pattern that differs from shot to shot both in the relative position of the peaks and in their visibility. The persistence of a periodic interference pattern even in the case of phase-uncorrelated sources is an effect essentially related to the limited number of emitters that interfere. Indeed, in the case of only two sources, even if there is no phase relation between them, one expects to observe a perfect interference pattern with 100% contrast [16]. Increasing the number of sources, the visibility of the peaks decreases and more complex structures start to grow. Even if the overall distribution still shows periodicity, the harmonic content of the interferogram grows at the expense of a reduced visibility and, in the limit of a very large number of sources, the interference pattern could be confused with noise. However, a correlation measurement should still be able to detect a periodic structure, that is closely related to the ordered distribution of the emitters. A detailed analysis of such a problem is carried out in [12].

In Fig. 5(c) we consider the case of coherent sources with a random displacement from their regular position $z_n = nd$. The interferogram on the right corresponds to the randomly generated set of displacements shown on the left. While in the case of random phases and uniform spacing a periodic interference pattern is still visible in a single shot, in the case of random spacing no characteristic structure is visible at all, even if all the sources emit coherently. This model reproduces the density distribution of a BEC released from a deep optical speckle potential, where a broad gaussian density profile, without any internal structure, has been experimentally observed [17].

4. Transport properties

In order to check the actual localization of the system in the regime of large lattice heights in which we observe interference fringes, we have studied dipole oscillations of the harmonically trapped BEC in the presence of the lattice. In order to induce dipole oscillations we suddenly shift the center of the magnetic trap over a distance Δz along the trap axis, as described in [2] with more detail. In Fig. 6 we show the center of mass position of the expanded cloud as a function of time for a trap displacement $\Delta z = 32 \mu\text{m}$ and different lattice heights. The black points refer to the regular undamped oscillation of the condensate in the pure harmonic potential at the trap frequency $\nu_z = (8.74 \pm 0.03) \text{ Hz}$.

The gray points correspond to the center-of-mass motion in a shallow lattice with $V_0 = 170$

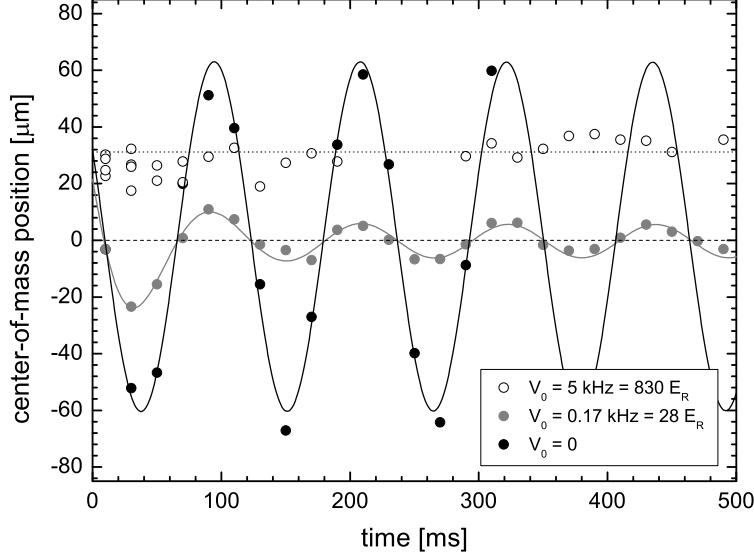


Fig. 6. Dipole oscillations of a harmonically trapped BEC in the presence of an optical lattice with $10 \mu\text{m}$ spacing. The dotted line is the initial position of the atoms at $t = 0$. The dashed line is the center of the magnetic trap after the excitation of the dipole mode. The black points refer to the oscillation without lattice, the gray points show a damped oscillation in a lattice with height $V_0 = 170 \text{ Hz}$, while the empty circles show the localization in a lattice with height $V_0 = 5 \text{ kHz}$.

$\text{Hz} = 28E_R$. In this case we observe a damped oscillation of the center of mass at the same frequency of the harmonic trap. This result is qualitatively different from what reported in [2], where the authors evidenced a frequency shift of the dipole oscillations in a standing wave lattice with $d \simeq 0.4 \mu\text{m}$. This shift was explained in terms of a modified effective mass m^* at the bottom of the energy band, which changes the frequency from v_z to $\sqrt{m/m^*}v_z$. Here the main difference is that, for a lattice spacing $d = 10 \mu\text{m}$ and a trap displacement $\Delta z = 32 \mu\text{m}$, the motion of the atomic cloud in momentum space is no longer confined in the center of the first Brillouin zone, where the band is approximately parabolic. Let us assume that the Bloch picture is still valid in this regime, in which the condensate occupies only ~ 15 sites. In Fig. 7(a) we show the band structure for a quantum particle in a periodic potential with spacing $d = 10 \mu\text{m}$. The solid line refers to a lattice height $V_0 = 28E_R$, while the dotted line shows the free particle parabolic spectrum. The width of the graph ($50\pi/d$) corresponds to the extension of the first Brillouin zone for a regular lattice with $0.4 \mu\text{m}$ spacing. Since now the lattice spacing is 25 times bigger, the corresponding width of the Brillouin zones π/d is 25 times smaller. Indeed, for the oscillation amplitudes we are considering, the atoms are spanning many Brillouin zones during their motion, making Landau-Zener tunnelling from one band to the next one at each passage from the zone edges. As a consequence, the actual energy spectrum probed by the atoms during the oscillation is basically the free particle one, with a curvature set by the real mass m , except for a small modification at the bottom, where small energy gaps form between the very first bands. The width of the gray region represents the actual range of momenta spanned by a particle oscillating in the pure harmonic trap for an initial displacement $\Delta z = 32 \mu\text{m}$. In Fig. 7(b) we show a zoom of the gray region, in which the thin continuous line represents the extension of the atomic wavepacket in momentum space

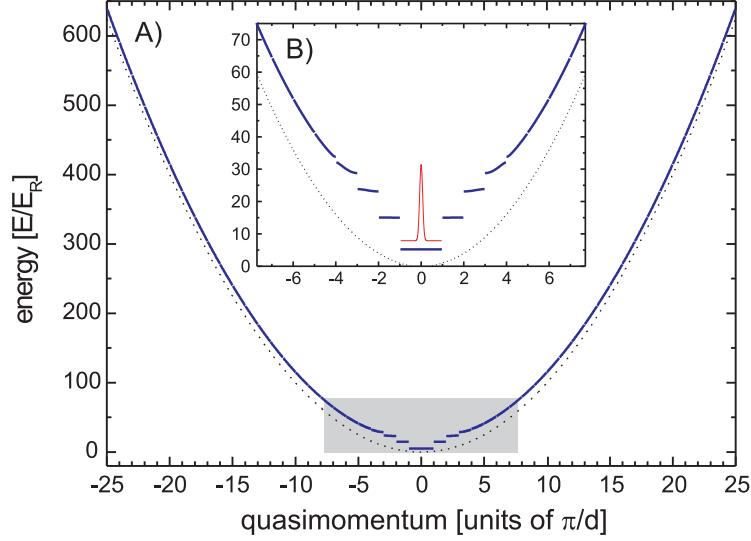


Fig. 7. a) Band structure for a quantum particle in a periodic potential with spacing $d = 10 \mu\text{m}$ for a lattice height $V_0 = 28E_R$ (solid line) and $V_0 = 0$ (dotted line). The width of the graph ($50\pi/d$) corresponds to the extension of the first Brillouin zone for a regular lattice with $0.4 \mu\text{m}$ spacing. b) Zoom of the gray box. The width of this graph is the actual range of momenta spanned by the atoms during the oscillation in the harmonic potential for the trap displacement $\Delta z = 32 \mu\text{m}$ used in the experiment. The thin line represents the extension of the atomic wavepacket in momentum space.

(its rms width being $0.07\pi/d$). In order to observe effects of reduced effective mass, like the ones studied in [2], one should use a much smaller amplitude oscillation ($\sim 1 \mu\text{m}$), that could be barely detectable with our imaging setup, in order to stay within one Brillouin zone. The observed damping of the center-of-mass oscillation could be attributed to the finite probability of interband Landau-Zener tunnelling during the motion of the wavepacket through the periodic potential. The splitting of the wavepacket into multiple bands then results in a dephasing of the different states leading to a damping of the center-of-mass motion. In addition, the finite transverse size of the lattice beam could play a role, causing the height of the optical barriers to be slightly different from site to site, thus breaking the exact translational symmetry of the lattice potential. In order to better understand which of these two mechanisms is more relevant for the observed dynamics further studies have to be carried out.

Coming back to Fig. 6, increasing the height of the optical lattice to $V_0 = 5 \text{ kHz} = 830E_R$, we observe that the center-of-mass motion is blocked and the atomic cloud stays at a side of the displaced harmonic trap. Indeed, in this regime the height of the periodic potential becomes larger than the chemical potential of the condensate and the BEC is split into an array of condensates located at the different sites. Differently from the standing wave lattice [2], in which the tunnelling ensures a collective motion even in the tight binding regime, in this case the tunnelling between adjacent sites is heavily suppressed by the large distance between wells, and the atomic states in each site are expected not to communicate one with each other. We note however that, even for this lattice height, we detect clear interference fringes as shown in Fig. 4(c) for all the evolution times considered in Fig. 6. The hypothesis of independence of the condensates localized at the lattice sites formulated before is thus confirmed by the observation

that, in the presence of an external potential gradient, the center of mass does not move in time.

We would like to note that this localization effect cannot be attributed to the generation of a Mott insulator state [3], as also suggested in [12]. Indeed, in the Mott insulator phase the system presents nontrivial localization properties on a timescale much longer than the tunnelling times. In our case the tunnelling is so heavily suppressed that the observation of the system is necessarily limited to a timescale on which the long-range coherence properties of the system could not be detected. Actually, what we are observing in the experiment is a localization effect produced only by the strongly increased tunnelling times, and not by an actual competition between interaction and tunnelling energies [3].

5. Conclusions

In this Letter we have presented a simple system for the production and detection of large-spacing optical lattices with adjustable spatial period. We have investigated transport and static properties of a Bose-Einstein condensate loaded in a periodic potential with $10\ \mu\text{m}$ spacing. In particular, we have evidenced the presence of interference fringes after expansion even in the insulating regime in which inter-well tunnelling is heavily suppressed and the center-of-mass dynamics is inhibited. The appeal of this system is that, by increasing the lattice spacing to $20\ \mu\text{m}$ or more, it becomes possible to optically resolve *in situ* the single lattice sites. This possibility could be important for the implementation of quantum computing schemes, where addressability is a fundamental requirement. As an extension of this work, the following step could be made in the direction of manipulating the single sites either optically or with the application of radiofrequency/microwave transitions coupling different internal levels.

Acknowledgements

This work has been supported by the EU Contracts No. HPRN-CT-2000-00125, INFM PRA “Photon Matter” and MIUR FIRB 2001. We thank all the people of the Quantum Gases group in Florence for stimulating discussions, in particular Michele Modugno for theoretical support and Vera Guarrera for careful reading of the manuscript.